Contrib Mineral Petrol (1997) 127: 17–29

Jonathan P Icenhower · David London

Partitioning of fluorine and chlorine between biotite and granitic melt: experimental calibration at 200 MPa H_2O

Received: 11 April 1996 / Accepted: 14 August 1996

Abstract Experiments from 640 to 680 °C, 200 MPa H_2O at $f_{O_2} \approx$ NNO, employing a natural F-rich vitrophyric rhyolite from Spor Mountain, Utah, assessed the effect of variable Mg′ [100Mg/(Mg + Mn + Fe)] on the partitioning of fluorine and chlorine between biotite (Bt) and melt. Over this temperature interval, Bt (± fluorite, ± quartz) is the sole liquidus phase. Partition coefficients for fluorine between biotite and glass ($D_F^{Bt/melt}$) show a strong dependence on the Mg′ of Bt. $D_F^{Bt/melt}$ varies from ~ 1.5 to 7.2 over the range of Mg′ from 21 to 76. A strong linear correlation between $D_F^{Bt/melt}$ and Mg′ has a slope of 9.4 and extrapolates through the origin (i.e., $D_F^{Bt/melt} \approx 0$ at Mg′ = 0, an annite-siderophyllite solid solution in these experiments). $D_{Cl}^{Bt/melt}$ values (~ 1 to 6) in the same experiments vary inversely with Mg′. The Al-content of biotite does not vary with the aluminum saturation index (ASI = molar Al_2O_3/ Σalkali and alkaline earth oxides) of melt, but two exchange mechanisms involving Al appear to operate in these micas: (1) $Al^{vi} + Al^{iv} \Leftrightarrow Si^{iv} + Mg^{vi}$, and $Mg^{vi} + 2Al^{iv} \Leftrightarrow 2Si^{iv} + \square^{vi}$. The effects of other components such as Li or other intensive parameters including f_{O_2} have yet to be evaluated systematically. At comparable Mg′ of Bt, however, the Spor Mountain rhyolite yields higher $D_F^{Bt/melt}$ values than an Li-rich, strongly peraluminous melt previously investigated. The results indicate that the Mg′ of Bt exerts the principal control on halogen partitioning, with ASI and *T* as second-order variables. The experimental partition coefficients compare well with other experimental results but not with most volcanic rocks. Magmatic Bt from most rhyolites records higher $D_F^{Bt/melt}$ due to reequilibration with degassed (H_2O-depleted) magma and perhaps with F_2O_{-1} exchange that may accompany oxidation ($[Fe^{3+}O]$ $[Fe^{2+}OH]_{-1}$). This behavior is evident in magmatic biotite from a zoned peraluminous rhyolite complex near Morococala, Bolivia: Bt is sharply zoned with F-rich rims, but Bt(core)-melt inclusion pairs fall on our experimental curve for $D_F^{Bt/melt}$. These experimental data can be used in part to assess the preservation of magmatic volatile contents in plutonic or volcanic silicic rocks. For plutonic rocks, the actual F-content of melt, not a relative activity ratio involving HF species, can be reasonably estimated if the mica has not undergone subsolidus reequilibration. This information is potentially useful for some shallow-level Ca-poor magmas that are thought to be rich in F (e.g., A- and S-type granites) but do not conserve F well as rocks.

J. P. Icenhower[1] · D. London (✉)
School of Geology & Geophysics University of Oklahoma
100 East Boyd Street,
SEC 810 Norman, OK 73019 USA

[1] *Present address*: Department of Geology, Geography, and Environmental Studies, Calvin College, Grand Rapids, Michigan (USA) 49546

Editorial responsibility: T. Grove

Introduction

Silicic rocks rich in fluorine have been reported by numerous investigators (e.g., Anfiligov et al. 1973; Burt et al. 1982; Christiansen et al. 1980, 1984; London 1987; Webster et al. 1987; Nash 1993). The prevailing model for the generation of these rocks, most of which are categorized as A-type (Whalen et al. 1987), entails melting of a dehydrated (and perhaps previously melted) protolith containing F-rich biotite. This model is based on the recognition of F-rich biotite in high-grade metamorphic terranes (e.g., Guidotti 1984), the observation that fluorine extends the stability of biotite to higher temperatures (Muñoz 1984; Peterson et al. 1991), and on the presumption that fluorine is strongly partitioned into biotite during episodes of partial melting. There are, however, reasons to suspect that fluorine does not partition into biotite as strongly as expected. Some granites (e.g., Cornwall, UK), pegmatites (e.g., San Diego County, CA), and rhyolites (e.g., Macusani, Peru) that are enriched in the volatile and incompatible elements Li, Cs, and B are also F-rich (London 1987). The magmas from which these rocks originated are mostly

characterized as S-type and are thought to be produced at relatively low temperatures from previously unmelted biotite-rich metasediments (e.g., Barbarin 1996). This association implies that substantial F may be transferred from mineral reservoirs to melt at the lower temperatures of incipient anatexis. Second, experimental investigations by Icenhower and London (1993, 1995) show that $D_F^{Bt/melt}$ is small for hydrous peraluminous melts (see also Skjerlie and Johnston 1992), resulting in F-rich melt produced at the earliest stages of partial melting.

The effects of F on melt properties and crystal-melt equilibria are substantial. For the granite system, these effects include lowering of liquidus and solidus temperatures, progressive shift in the normative silica content of crystallizing melts, reduced viscosity, possibly increased H_2O content of melt and important interactions with some high field-strength elements (e.g., Manning 1981; Dingwell 1985, 1987; Keppler 1993). Though there is ample reason to want to know the actual F content of magma, many granites, pegmatites, and rhyolites do not conserve their fluorine concentrations (London 1987). The experimental calibration of $D_F^{Bt/vapor}$ (Muñoz and Ludington 1974) remains the most widely used method to establish a qualitative measure of enrichment of F in vapor that coexists with biotite, but it applies strictly to crystal-vapor equilibria and should not be extended to equilibria between biotite and melt (though it has by others). Additionally, the parameter calculated is for this exchange (Muñoz and Ludington 1974) is the component HF, which is thought to represent a negligible fraction of the total F in a hydrous alkali aluminosilicate melt (e.g., Schaller et al. 1992). We provide an illustration of the disparity between the F content of melt calculated by (the misuse of) the method of Muñoz and Ludington (1974) and the actual measured F content of melt.

As an extension of the preliminary investigations by Icenhower and London (1993, 1995), this paper presents new partitioning data determined by experiment on the Spor Mountain rhyolite, a slightly peraluminous F-enriched vitrophyre from Utah (cf. Webster et al. 1987). We determined values of $D_F^{Bt/melt}$ on experimentally grown biotite over the temperature interval of 640 to 680 °C at 200 MPa H_2O pressure. We have also determined values of $D_{Cl}^{Bt/melt}$ in the same experiments, though for reasons explained below not as fully as for F.

Spectroscopic and theoretical studies predict and find Fe-F avoidance and Mg-F affinity in the octahedral layers of biotite solid solutions (e.g., Kalinichenko et al. 1975; Sans and Stone 1983; Mason 1992); thus, $D_F^{Bt/melt}$ should be governed by the Mg′ of biotite. The converse behavior apparently is true for Cl (e.g., Mason 1992). In these experiments, therefore, the principal variable was Mg′ [= 100Mg/(Mg + Mn + Fe)] of biotite, which was manipulated between 21 and 76 by small additions of Fe- or Mg-rich components. Our experimental results confirm a correlation between $D_F^{Bt/melt}$ $D_{Cl}^{Bt/melt}$ with Mg′ of biotite. Though Mg′ appears to be the most important control on $D_F^{Bt/melt}$, we are currently extending this work to assess the second-order effects of aluminum saturation index (ASI = molar Al_2O_3/Σ alkali and alkaline earth oxides) of melt and Fe^{3+}/Fe^{T} of biotite (indirectly f_{O_2} of melt).

Experimental methods

Starting material was a -200 mesh sample of vitrophyric rhyolite from Spor Mountain, Utah (SM-1 of Webster et al. 1987, kindly provided by Jim Webster). According to Webster et al. (1987), SM-1 consists of 70% glass and 30% crystals. The Mg′ of SM-1 reported by these investigators is zero (0.00 wt% MgO), so that glasses of synthetic pyrope or phlogopite or natural crystalline forsterite (Kilbourne Hole, New Mexico, Table 1) were added to increase Mg′ of melt and resultant biotite (but note that the unadulterated sample of SM-1 used here yielded biotite with Mg′ of ~ 30). Approximately 20 mg rock powder and ~ 2 mg distilled water were sealed into Au capsules measuring 1 cm × 3 mm, with the rock/water mix confined to the central 5 mm of the capsule. Following drying and checks for leaks, successfully sealed capsules were run in René-41 cold-seal reaction vessels with Hastelloy-C filler rods and run at 200 MPa. The pressure medium was water plus trace amounts of a hydrocarbon-based rust inhibitor that imposed an oxygen fugacity slightly less than the NNO buffer of the reaction vessel (Huebner 1971). Experiments were of sufficient duration and temperature to establish equilibration of f_{O_2} by diffusion of H_2 between experiment and the pressure reservoir across Au tubing of 0.18 mm thickness (Chou 1987). Pressure was monitored by a factory-calibrated Heise Bourdon-tube gauge, and all experiments were conducted open to the gauge and a 2-liter pressure buffer; pressure uncertainty is < 1MPa. Temperatures were monitored by internal Chromel-Alumel thermocouples; temperature uncertainty (gradient + thermocouple accuracy) is ± 4 °C. Experiments were quenched isobarically in an air jet to < 300 °C in 10-50 seconds. Capsules were weighed after runs to check for leaks; however, all capsules gained weight (≈ 0.2 mg) due to diffusion of Ni from the reaction vessel into the capsule. Run products were analyzed by optical examination, scanning (SEM) and backscattered electron (BSE) imaging, and energy (EDS)- and wavelength (WDS)-dispersive X-ray spectrometry. Quantitative analyses of run products were exclusively performed using WDS techniques. Analytical conditions for electron microprobe analysis (EMPA), including beam conditions and lower limits of detection (L.L.Ds), are tabulated in the Appendix. Biotite crystals selected for analysis were oriented such that the [100] zonal plane was parallel to the electron beam so that analyses penetrated the direction of maximum thickness in the biotite, and any variations in X-ray counting yields based on beam-crystal orientation were eliminated.

All capsules were taken to a temperature of 750 °C, which is close to the liquidus of the water-saturated system at 200 MPa

Table 1 Summary of additives to Spor Mountain base composition

Compositions with pyrope gel
GA1: 0.5 wt% Mgo
GA2: 1.0 wt% MgO
GA3: 0.2 wt% MgO
Compositions with phlogopite gel
PH1: 0.5 wt% MgO
PH2: 1.0 wt% MgO
Compositions with 2 wt% RbCl solution
GA3-4: 8.6 wt% of solution
GA3-5: 20.6 wt% of solution
Compositions with seed crystals
SM-7: Fe filings
SM-12: Forsterite seeds

(Webster et al. 1987), for three days and then cooled to the temperature of interest. Control experiments quenched from 750 °C contained essentially all glass. Experiments were first cooled to 680 °C for one day, where biotite is the liquidus phase (Webster et al. 1987), followed by 20 °C cooling steps on subsequent days to the final temperatures of 660, 640, 600 and 580 °C. Durations of experiments were mostly 1 month at the final temperature; this duration was sufficient to produce homogeneity of glass and biotite and a textural steady-state of biotite grain size. We take the homogeneity of melt and biotite, the steady-state attainment of biotite grain size and morphology, and lack of other reaction relationships to represent a close approach to mineral-melt equilibrium. We have noted in previous work (Icenhower and London 1995) that strict reversals of partitioning, which are accomplished through exchange by diffusion, do not work for micas – micas, even those close to the equilibrium composition, react readily with melt by dissolution and reprecipitation of the new phase. Thus, all such experiments amount to synthesis reactions, but the tendency of micas to recrystallize readily, quickly, and completely implies that the crystals are close to their compositions in equilibrium with melt.

Concentrations of Cl are low in SM-1 (0.15 wt%: Webster and Holloway 1988), which is below the saturation limit of ~ 0.25 (Webster 1992). In order to enhance EMPA of Cl in both glass and biotite, we added aqueous solutions containing either RbCl or KCl-NaCl mixtures to selected starting compositions. Concentrations of added Cl varied from relatively low (≈ 0.2 wt%) to high (2 wt%). As we discuss below, only the experiments with relatively low concentrations of Cl contained biotite.

Results

The charges contained glass (= quenched melt) and biotite laths with fluorite, quartz, and zircon noted in several charges. Biotite crystallized as sharply hexagonal prisms or laths (Fig. 1). Fluorite formed euhedral cubes or dodecahedra that fluoresced brightly under the electron beam. By EDS, the fluorite contained high concentrations of yttrium. In some experiments, halite crystals have precipitated along fractures that intersect the surface of glass; the halite presumably originates from aqueous fluids in vesicles that ruptured below the surface after the charge was polished. Experiments cooled to less than 640 °C (600 and 580 °C) contained plagioclase, quartz, and sanidine in addition to biotite, consistent with the phase relations reported by Webster et al. (1987). Biotite in the lower-temperature runs, however, was too fine-grained for accurate EMPA. Bulk compositions containing > ~0.5 wt% added Cl did not yield biotite at any *T*. Fluids released from punctured capsules deposited a pink to red precipitate that we infer to be iron chloride. An affinity of Cl for Fe (e.g., Barnes 1979) apparently leached the little Fe from melt into vapor and so destabilized biotite.

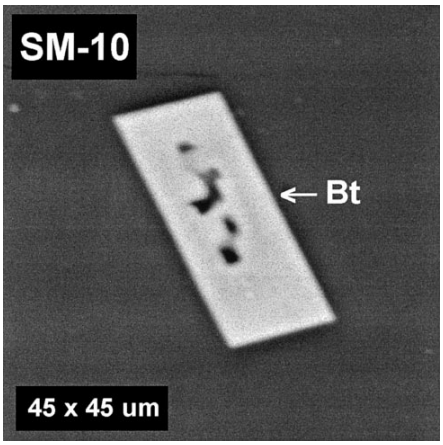

Fig. 1 Back-scattered electron micrograph of experimental SM-10 showing a typical crystal of biotite (size, orientation) that would have been a target for EMPA

Glass

Compositions of glasses are tabulated in Table 2. The glasses were analyzed by a 15-μm fixed beam at two different conditions: Na, K, Si, and Al by a 2 nA beam current and 20 kV potential, and Ti, Mg, Ca, Mn, Fe, Ni, Cs, Rb, and F with a 20 nA beam current, 20 kV potential. A subset of experiments used a routine in which Cl was determined instead of NiO. Details of the analytical routine are given in the Appendix.

In general, the glasses are highly silicic and contain corundum in the norm indicating peraluminous compositions. The excess Al content is assessed through the aluminum saturation index (ASI = molar Al_2O_3/Σ alkali and alkaline earth oxides), which varies mostly between 1.12 and 1.20 for these experiments. The more peraluminous compositions result in part from loss of alkalis with chloride to vapor in some doped experiments, and from the addition of synthetic pyrope gel in other experiments.

The sum of the femic components (TiO_2, MgO, MnO, NiO, and FeO) are below 1 wt% for all glasses, with TiO_2, MgO, and NiO typically below detection limit. Average K′ [= molar $100K_2O/(Na_2O + K_2O)$] is 46, with Rb_2O slightly above the detection limit. Concentrations of SrO, BaO and Cs_2O are all below their respective detection limits. Fluorine concentrations are relatively high with values ranging between 0.8 and 1.8 wt%. Experiments without added Cl contain approximately 0.05 wt% Cl in glass. Experiments with the RbCl solution yield glasses that contain 0.07 (GA3-5) and 0.20 (GA3-4) wt% Cl (and ASI = 1.27).

Biotite

Compositions of biotite are shown in Table 3. All analyses are recalculated on the basis of 24 O, F and Cl. Total iron is reported as FeO.

The number of Al^{iv} cations is defined as the difference between the number of tetrahedral cations (8) and the measured number of silicon atoms per formula unit (p.f.u.) and varies between ~1.6 and 2.2. By definition, the number of Al^{iv} atoms diminishes as the biotite becomes more siliceous. Biotite from undoped experiments contains < 6.00 Si atoms p.f.u.. Experiments with added phlogopite or pyrope gels, however, yielded biotite with

Table 2 Glass compositions[a]

Run Temp #Analyses	SM-11 640 n=20	Std Error	SM-7 660 n=19	Std Error	SM-10 660 n=20	Std Error	SM-9 680 n=19	Std Error	SM-13 680 n = 21	Std Error	GA1-2 640 n=19	Std Error	SM-12 660 n=20	Std Error
SiO_2	70.14	(0.10)	69.60	(0.17)	70.08	(0.05)	69.93	(0.11)	70.04	(0.15)	69.18	(0.12)	69.96	(0.13)
TiO_2	0.04	(0.01)	*0.04*		*0.04*		*0.04*		*0.04*		*0.04*		*0.04*	
Al_2O_3	13.74	(0.05)	13.78	(0.08)	13.69	(0.04)	13.44	(0.07)	13.45	(0.08)	13.29	(0.05)	13.72	(0.04)
MgO	*0.02*		*0.02*		*0.02*		*0.02*		*0.02*				*0.02*	
CaO	0.40	(0.01)	0.38	(0.01)	0.39	(0.01)	0.43	(0.01)	0.45	(0.01)	0.42	(0.01)	0.46	(0.01)
MnO	0.04	(0.01)	0.04	(0.01)	0.05	(0.00)	0.05	(0.01)	0.04	(0.01)	0.03	(0.00)	0.03	(0.01)
FeO[b]	0.35	(0.01)	0.47	(0.01)	0.45	(0.01)	0.55	(0.01)	0.53	(0.01)	0.34	(0.04)	0.35	(0.02)
NiO			*0.04*						*0.04*					
SrO	*0.07*		*0.07*		*0.07*		*0.07*		*0.07*		*0.07*		*0.07*	
BaO	*0.13*		*0.13*		*0.13*		*0.13*		*0.13*		*0.13*		*0.13*	
Na_2O	3.69	(0.04)	3.91	(0.03)	3.82	(0.03)	3.61	(0.03)	3.62	(0.04)	3.68	(0.05)	3.62	(0.04)
K_2O	4.77	(0.02)	4.75	(0.02)	4.67	(0.02)	4.73	(0.03)	4.54	(0.02)	4.26	(0.03)	4.68	(0.02)
Rb_2O	0.09	(0.01)	0.06	(0.01)	0.09	(0.01)	0.05	(0.01)	0.05	(0.01)	0.08	(0.01)	0.07	(0.01)
Cs_2O	*0.11*		*0.11*		*0.11*		*0.11*		*0.11*		*0.11*		*0.11*	
F	1.80	(0.13)	1.59	(0.09)	1.60	(0.07)	1.81	(0.11)	1.56	(0.10)	0.99	(0.04)	1.43	(0.08)
Cl	0.05	(0.01)			0.06	(0.01)	0.06	(0.01)			0.06	(0.01)	0.06	(0.01)
Total	95.42		94.96		95.24		95.00		94.68		92.72		94.72	
O≡F, Cl	94.65		94.31		94.55		94.23		94.02		92.29		94.11	
ASI[c]	1.15		1.12		1.13		1.13		1.15		1.16		1.16	

[a]Italics = detection limit, blank = not determined.
[b]All Fe as FeO.
[c]ASI = molar Al/(Ca + Na + K + Rb).

Si contents between 5.83 to 6.36 atoms p.f.u. The Si contents for these latter experiments are high but within the range of values reported in both natural (Robert and Maury 1979) and experimental (Puziewicz and Johannes 1990) biotite. The occupancy of the tetrahedral site has no effect on F partitioning (e.g., Mason 1992).

The number of Al^{vi} cations is taken as the difference between the total number of Al atoms and Al^{iv} atoms. The total Al in biotite from these experiments (2.2 to 2.7 p.f.u.) shows no meaningful variation with increasing ASI of melt. The total Al-content of the biotite also is low but overlaps with biotite compositions in some peraluminous granites (e.g., Villaseca and Barbero 1994) and matches biotite compositions in nearly identical experiments (e.g., Puziewicz and Johannes 1990; f_{O_2} = NNO, water saturated, 200 MPa pressure, moderately peraluminous melt). The number of Fe atoms p.f.u. varies between 1.2 to 4.1 and inversely with Mg (1.1 to 4.0 atoms p.f.u.). A deficit of octahedral cations (Table 2) probably stems from two sources. Silicon in excess of 6 cations p.f.u. is accommodated by the exchange

$$Mg^{vi} + 2Al^{iv} \Leftrightarrow 2Si^{iv} + \square^{vi} \text{(Seifert and Schreyer 1971)}, \quad (1)$$

which is applicable to the more magnesian micas listed in Table 2. Octahedral site occupancy will also be underestimated by calculating all Fe as FeO. Because of the probable operation of substitution 1 and uncertainties in the distribution of Fe^{3+} between octahedral and tetrahedral sites (e.g., Dyar 1990) we have not estimated the Fe^{3+}/Fe^{T} from site occupancy deficits. We expect the Fe^{3+}/Fe^{T} ratio of the experimentally grown biotite to be near 15%, as explained in discussion section below.

Values of Mg′ [= 100Mg/(Mg + Mn + Fe)] in biotite were manipulated between 21 to 76 spanning compositions from annite to phlogopite; siderophyllite and eastonite components are low in all experimental biotite (Fig. 2A). Concentrations of silicon increase with increasing values of Mg′, suggesting that the substitution of Mg for Fe is coupled with aluminum-silica substitutions on the tetrahedral and octahedral site (i.e., Tschermak substitution):

$$^{vi}(Mg, Fe)^{2+} + {}^{iv}Si^{4+} = {}^{vi}Al^{3+} + {}^{iv}Al^{3+} \quad (2)$$

As displayed in Fig. 2B, this substitution appears to exert the dominant control over the biotite compositions. Similar variations have been observed in peraluminous granite suites (e.g., Villaseca and Barbero 1994).

Partition coefficients

Fluorine

Mineral/melt partition coefficients, or $D_M^{Bt/glass}$ where M is either F or Cl, are determined by dividing the concentration of the halogen in biotite by its concentration in glass. Halogen (F, Cl) partition coefficient values for each experiment are tabulated in Table 4. The striking feature in this table is the strong correlation between $D_F^{Bt/melt}$ and Mg′ of biotite, which is revealed in a plot of $D_F^{Bt/melt}$ and Mg′ of biotite with 2σ error bars (standard deviation about the mean) included (Fig. 3A). The line of least squares fit regressed through the data indicates a slope of 9.4 and an intercept that passes close to the origin.

GA1-1 680 n=20	Std Error	GA2-2 640 n=19	Std Error	GA2-1 680 n=20	Std Error	PH1-1 640 n=20	Std Error	PH2-1 680 n=19	Std Error	GA3-4 680 n=34	Std Error	GA3-5 680 n=25	Std Error
69.85	(0.10)	70.10	(0.12)	69.70	(0.11)	69.48	(0.13)	69.91	(0.14)	66.70	(0.30)	68.89	(0.05)
0.04		*0.04*		*0.04*		*0.04*		*0.04*		*0.04*		*0.04*	
13.18	(0.06)	13.42	(0.02)	12.94	(0.03)	13.08	(0.04)	13.15	(0.03)	13.52	(0.03)	13.39	(0.02)
0.03	(0.00)	0.05	(0.02)	0.11	(0.04)	0.04	(0.00)	0.03	(0.00)	*0.02*		*0.02*	
0.41	(0.01)	0.42	(0.01)	0.42	(0.00)	0.42	(0.01)	0.42	(0.00)	0.47	(0.01)	0.43	(0.01)
0.04	(0.00)	0.04	(0.02)	0.04	(0.00)	0.04	(0.00)	0.04	(0.00)	0.04	(0.00)	0.04	(0.00)
0.37	(0.01)	0.26	(0.02)	0.36	(0.03)	0.42	(0.01)	0.33	(0.00)	0.46	(0.00)	0.42	(0.00)
0.04						*0.04*		*0.04*					
0.07		*0.07*		*0.07*		*0.07*		*0.07*		*0.07*		*0.07*	
0.13		*0.13*		*0.13*		*0.13*		*0.13*		*0.13*		*0.13*	
3.49	(0.04)	3.54	(0.04)	3.39	(0.05)	3.55	(0.04)	3.71	(0.04)	3.72	(0.04)	3.05	(0.26)
4.33	(0.02)	4.13	(0.03)	4.07	(0.02)	4.55	(0.02)	4.47	(0.03)	4.54	(0.02)	4.36	(0.05)
0.08	(0.01)	0.08	(0.01)	0.07	(0.00)	0.08	(0.01)	0.07	(0.01)	0.27	(0.01)	0.86	(0.03)
0.11		*0.11*		*0.11*		*0.11*		*0.11*		*0.11*		*0.11*	
1.06	(0.03)	0.83	(0.01)	0.95	(0.03)	1.02	(0.02)	0.88	(0.02)	1.95	(0.01)	0.98	(0.01)
		0.05	(0.01)	0.06	(0.01)					0.19	(0.01)	0.07	(0.01)
93.22		93.25		92.43		93.06		93.39		91.31		92.64	
92.77		92.89		92.02		92.63		93.02		90.78		92.20	
1.18		1.21		1.20		1.13		1.12		1.16		1.27	

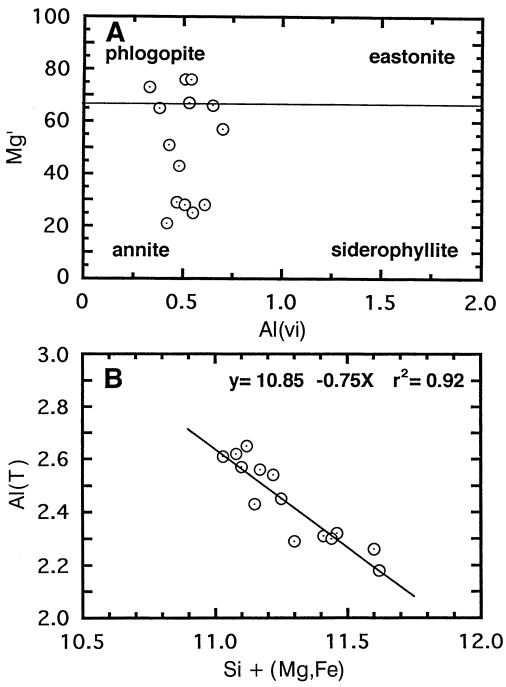

Fig. 2A Plot of biotite compositions from our experiments on the biotite quadrilateral. This figure illustrates that the biotite compositions are dominantely annite-phlogopite mixtures. **B** Plot of total aluminum (cations) versus the sum of Si, Mg, and Fe (cations) in biotite. A line of least squares fit regressed through the data indicates that reaction 2 is the dominant exchange mechanism in the biotite (see text)

Figure 3B displays the values of $D_F^{Bt/melt}$ versus temperature for constant values of Mg′. Experiments grouped in this way appear to indicate a slight negative correlation between $D_F^{Bt/melt}$ and T, albeit over a narrow range of T (cf., Icenhower and London 1995). Fig. 4A shows that total Al in biotite does not increase with ASI of melt; Fig. 4B illustrates that total Al in biotite decreases with increasing $D_F^{Bt/melt}$, as expected from the exchange reaction 2. The operation of exchange reaction 2 should increase the ASI of coexisting melt; this is seen in Fig. 4C, though the correlation of data about a linear regression of the mean is not strong. Among all of these variables, the Mg′ of biotite is clearly the most important parameter in fluorine partitioning.

Chlorine

Figure 5 illustrates that values of $D_{Cl}^{Bt/melt}$ plotted against Mg′ show an inverse correlation. At low values of Mg′ (30) $D_{Cl}^{Bt/melt}$ varies between 3 and 6, but approaches unity at higher Mg′ values (70). Although not as well correlated as $D_F^{Bt/melt}$, these data corroborate Mg-Cl avoidance (e.g., Mason 1992). The data also indicate that Mg′ governs Cl partitioning between biotite and melt.

Discussion

Octahedral site occupancy and $D_F^{Bt/melt}$

The compositions of biotite synthesized here lie within natural bounds, albeit with Mg-rich micas containing elevated Si. As $D_F^{Bt/melt}$ is a function of octahedral site occupancy (Mason 1992), it becomes critical to

Table 3 Biotite compositions[a]

Temp	640		660		680		680		680		640		660	
Run	SM-11	Std	SM-7	Std	SM-10	Std	SM-9	Std	SM-13	Std	GA1-2	Std	SM-12	Std
#Analyses	n=10	Error	n=12	Error	n=19	Error	n=11	Error	n=10	Error	n=10	Error	n=3	Error
SiO_2	38.12	(0.46)	38.53	(0.25)	37.51	(0.28)	37.69	(0.35)	37.42	(0.33)	42.31	(0.12)	42.73	(0.55)
TiO_2	0.65	(0.08)	0.99	(0.13)	0.70	(0.06)	0.78	(0.17)	0.77	(0.07)	0.37	(0.03)	0.43	(0.02)
Al_2O_3	14.06	(0.20)	13.50	(0.22)	13.63	(0.14)	13.85	(0.30)	14.05	(0.16)	13.32	(0.04)	14.03	(0.01)
MgO	6.09	(0.28)	4.58	(0.19)	6.56	(0.36)	6.26	(0.53)	5.47	(0.25)	15.78	(0.09)	12.77	(0.07)
CaO	*0.03*		*0.02*		*0.02*		0.03	(0.01)	*0.02*		*0.02*		0.04	(0.01)
MnO	0.78	(0.01)	0.51	(0.02)	0.65	(0.01)	0.62	(0.02)	0.62	(0.01)	0.33	(0.00)	0.48	(0.02)
FeO[b]	26.59	(0.22)	30.86	(0.28)	27.62	(0.43)	27.48	(0.74)	28.51	(0.38)	13.75	(0.11)	16.50	(0.39)
NiO	*0.07*	(0.01)	*0.04*		*0.04*		0.12	(0.04)	*0.04*		*0.04*		0.06	(0.01)
SrO	*0.07*		*0.07*		*0.07*		*0.07*		*0.07*		*0.07*		*0.07*	
BaO	*0.13*		*0.13*		*0.13*		*0.13*		*0.13*		*0.13*		*0.13*	
Na_2O	0.48	(0.05)	0.40	(0.03)	0.38	(0.02)	0.40	(0.02)	0.38	(0.02)	0.64	(0.01)	0.55	(0.03)
K_2O	8.62	(0.06)	8.52	(0.03)	8.76	(0.05)	8.67	(0.05)	8.53	(0.06)	8.94	(0.02)	8.79	(0.09)
Rb_2O	0.17	(0.03)	0.13	(0.01)	0.12	(0.01)	0.10	(0.02)	0.16	(0.01)	0.17	(0.00)	0.19	(0.01)
Cs_2O	*0.11*		*0.11*		*0.11*		*0.11*		*0.11*		*0.11*		*0.11*	
H_2O	2.23	(0.06)	2.45	(0.04)	2.01	(0.04)	2.14	(0.07)	2.47	(0.04)	1.19	(0.02)	1.74	(0.04)
F	3.08	(0.09)	2.51	(0.07)	3.49	(0.10)	3.27	(0.18)	2.57	(0.07)	5.62	(0.04)	4.56	(0.12)
Cl	0.15	(0.07)			0.17	(0.10)	0.38	(0.02)			0.09	(0.01)	0.07	(0.02)
Total	100.97		101.00		101.43		101.41		100.95		102.42		102.87	
O≡F, Cl	99.64		99.94		99.92		99.95		99.87		100.03		100.93	
	Cations (abridged) on the basis of 24 O, F, Cl													
Si	6.00		5.86		5.93		5.94		5.93		6.22		6.27	
^{iv}Al	2.00		2.14		2.07		2.06		2.07		1.78		1.73	
^{vi}Al	0.61		0.42		0.47		0.51		0.55		0.53		0.70	
Ti	0.08		0.12		0.08		0.09		0.09		0.04		0.05	
Mg	1.43		1.10		1.55		1.47		1.29		3.46		2.79	
Mn	0.10		0.07		0.09		0.08		0.08		0.04		0.06	
Fe	3.50		4.14		3.65		3.62		3.78		1.69		2.03	
Na	0.15		0.12		0.12		0.12		0.12		0.18		0.16	
K	1.73		1.74		1.77		1.74		1.72		1.68		1.65	
Rb	0.02		0.01		0.01		0.01		0.02		0.02		0.02	
OH	2.34		2.62		2.12		2.25		2.61		1.17		1.70	
F	1.53		1.27		1.74		1.63		1.29		2.61		2.12	
Cl	0.04				0.05		0.10				0.02		0.02	
Cation														
Total	15.62		15.72		15.74		15.64		15.65		15.64		15.46	
Mg′[d]	28	(4)	21	(3)	29	(7)	28	(4)	25	(4)	67	(1)	57	(2)

[a]Italics = detection limit, blank = not determined.
[b]All Fe as FeO.
[c]H_2O on the basis of stoichiometry.
[d]$Mg' = 100 \times Mg/(Mg + Mn + Fe)$.

Table 4 Summary of partition coefficients and biotite and melt compositions (numbers in parentheses are the standard errors)

Experiment	$D_F^{Bt/melt}$	$D_{Cl}^{Bt/melt}$	Mg′	ASI
SM-11	1.71(0.58)	2.97(1.54)	28(4)	1.15
SM-7	1.59(0.42)		21(3)	1.12
SM-10	2.18(0.51)	2.86(1.76)	29(7)	1.13
SM-9	1.81(0.51)	6.25(1.10)	28(4)	1.13
SM-13	1.65(0.52)		25(4)	1.15
GA1–2	5.68(0.18)	1.53(0.36)	67(1)	1.16
SM-12	3.19(0.14)	1.22(0.34)	57(2)	1.16
GA1–1	5.10(0.22)		66(2)	1.21
GA2–2	7.19(0.50)		76(5)	1.21
GA2–1	6.27(0.20)	1.40(0.46)	76(2)	1.20
PH1–1	5.43(0.76)		65(6)	1.13
PH2–1	6.58(0.67)		73(2)	1.12
GA3–5	3.93(0.33)	3.43(0.61)	51(6)	1.27
GA3–4	3.50(0.11)	2.06(0.27)	43(2)	1.16

determine the composition of the octahedral layer in order to understand the crystallographic controls on F-Cl-OH substitution. The relations of F content to variations in Mg′ (e.g., Mason 1992) and even Al^{vi} (e.g., Muñoz 1984) are reasonably well defined. The strengths of correlations (R^2) shown in Fig. 3A (Mg′) and 2B (Al^{vi}) demonstrate smooth and systematic variations of biotite compositions with changes in the composition of the system, and that these variables – Mg′ in particular – control $D_F^{Bt/melt}$.

The effects of octahedral vacancies such as those generated by substitution 2 are unknown, but the fraction of $\square^{vi}$, which is equivalent to half the molar Si above 6 atoms p.f.u., is small for all biotite synthesized here (Table 2). The Fe^{3+}/Fe^T and the distribution of Fe^{3+} between octahedral and tetrahedral sites in the biotite probably represent more significant uncertainties.

660 GA1-1 n=10	Std Error	640 GA2-2 n=12	Std Error	680 GA2-1 n=8	Std Error	640 PH1-1 n=7	Std Error	680 PH2-1 n=4	Std Error	680 GA3-5 n=13	Std Error	680 GA3-4 n=9	Std Error
43.38	(0.10)	43.10	(0.38)	43.16	(0.26)	41.02	(0.51)	42.25	(0.63)	38.39	(0.41)	37.01	(0.81)
0.35	(0.01)	0.26	(0.05)	0.25	(0.02)	0.52	(0.11)	0.55	(0.06)	1.06	(0.26)	1.03	(0.02)
13.24	(0.03)	13.71	(0.15)	13.48	(0.05)	12.90	(0.16)	12.65	(0.21)	13.34	(0.12)	14.29	(0.25)
14.96	(0.12)	18.76	(0.27)	18.42	(0.25)	15.93	(0.48)	18.47	(0.19)	11.59	(0.47)	9.66	(0.02)
0.03		*0.03*		*0.03*		*0.03*		*0.03*		0.09	(0.07)	0.04	(0.04)
0.36	(0.01)	0.24	(0.01)	0.24	(0.00)	0.43	(0.02)	0.33	(0.03)	0.48	(0.02)	0.50	(0.06)
13.32	(0.09)	10.26	(0.36)	9.91	(0.13)	15.16	(0.37)	11.69	(0.38)	19.37	(0.75)	22.37	(0.81)
0.04		*0.04*		*0.04*		*0.04*		*0.04*					
0.07		*0.07*		*0.07*		*0.07*		*0.07*		*0.07*		*0.07*	
0.13		*0.13*		*0.13*		*0.13*		*0.13*		*0.13*		*0.13*	
0.65	(0.01)	0.63	(0.02)	0.61	(0.01)	0.53	(0.03)	0.53	(0.05)	0.41	(0.03)	0.69	(0.19)
8.59	(0.03)	9.08	(0.08)	9.05	(0.04)	9.19	(0.06)	9.26	(0.07)	7.92	(0.04)	8.53	(0.01)
0.17	(0.00)	0.18	(0.01)	0.16	(0.01)	0.16	(0.00)	0.15	(0.01)	1.59	(0.09)	0.35	(0.06)
0.11		*0.11*		*0.11*		*0.11*		*0.11*		*0.11*		*0.11*	
1.31	(0.03)	1.11	(0.06)	1.09	(0.04)	1.00	(0.17)	1.15	(0.06)	1.84	(0.04)	1.79	(0.10)
5.41	(0.06)	5.97	(0.12)	5.96	(0.06)	5.54	(0.21)	5.79	(0.12)	3.85	(0.06)	3.67	(0.21)
				0.08	(0.02)					0.22	(0.02)	0.39	(0.08)
101.74		103.30		102.33		102.38		102.82		100.13		100.30	
99.46		100.79		99.82		100.05		100.38		98.51		98.75	
6.36		6.19		6.24		6.12		6.15		5.98		5.83	
1.64		1.81		1.76		1.88		1.85		2.02		2.17	
0.65		0.51		0.54		0.38		0.33		0.43		0.48	
0.40		0.03		0.03		0.06		0.06		0.12		0.12	
3.27		4.01		3.97		3.54		4.01		2.69		2.27	
0.04		0.03		0.03		0.05		0.04		0.06		0.07	
1.63		1.23		1.20		1.89		1.42		2.52		2.95	
0.18		0.18		0.17		0.15		0.15		0.12		0.21	
1.61		1.66		1.67		1.75		1.72		1.57		1.71	
0.02		0.02		0.03		0.04		0.01		0.16		0.04	
1.28		1.06		1.05		0.99		1.12		1.91		1.88	
2.51		2.71		2.73		2.61		2.67		1.90		1.83	
				0.02						0.06		0.10	
15.80		15.67		15.62		15.84		15.74		15.67		15.85	
66	(2)	76	(5)	76	(2)	65	(6)	73	(2)	51	(6)	43	(2)

The ratio Fe^{3+}/Fe^{T} in rhyolite melt at ≤ 700 °C, 200 MPa H_2O, and f_{O_2} = NNO is ≤ 0.1 (Baker and Rutherford 1996). Melts produced here are nearly identical in composition and imposed conditions and hence should have a similarly low Fe^{3+}/Fe^{T}. Biotite spanning a range of Mg′ synthesized at NNO in more alkaline melt contains ~ 15% Fe^{3+}/Fe^{T} (Righter and Carmichael 1996). Annite synthesized at reducing (≤ FMQ) and more oxidizing (≥ NNO) conditions contains 5 and 15% Fe^{3+}, respectively (Redhammer et al. 1993; Dachs 1994; Dachs and Benisek 1995). We conclude that the biotite synthesized in our experiments will contain between 10 and 15% Fe^{3+}/Fe^{T}, and a substantial portion of the Fe^{3+} may occupy tetrahedral sites (e.g., Dyar 1990). Consequently, the Fe^{3+}/Fe^{T} should be low, close to the annite-eastonite join, and whatever the effect of $^{vi}Fe^{3+}$ on $D_F^{Bt/melt}$, it should be negligible in these experimental results.

Deviations from perfect Fe-F avoidance, manifested as F in excess of that predicted by Muñoz and Ludington (1974) for a given component of biotite, have been attributed to nonideal mixing of components on the (OH, F, Cl) site (e.g., Finch et al. 1995) and to short-range order by clustering of octahedral Fe^{2+} and Mg (e.g., Sanz and Stone 1983; Zhu and Sverjensky 1992; Mason 1992). Our experimental data fit a simple linear mixing relation of Fe-F avoidance that would be consistent with ideal mixing on both the octahedral (Fe, Mg) site and the (OH, F, Cl) site at low Cl contents (see Zhu and Sverjensky 1992). We suggest that one problem with any interpretive analysis of the existing data (natural or synthetic mica) is the general lack of analysis of Fe^{3+}/Fe^{T} in the biotite, i.e., that the "annite" component may be incorrectly estimated from structural analyses based on EMPA.

$D_F^{Bt/melt}$ in Li-rich peraluminous melt

At comparable Mg′, $D_F^{Bt/melt}$ appears to be lower (than results here) in Li-rich and strongly peraluminous melt (ASI = 1.3 to 1.4) generated by the hydrous anatexis of

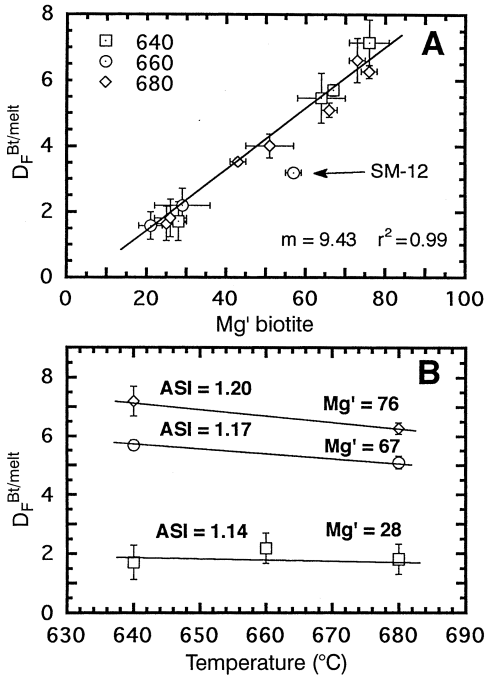

Fig. 3A Plot of $D_F^{Bt/glass}$ versus Mg′ in biotite for the Spor Mountain experiments. A least squares fit line regressed through the data passes close to the origin. One data point (SM-12) lies off of the correlation because the experiment failed to reach equilibrium, as indicated by unstable but relic forsterite seed crystals. **B** Plot of $D_F^{Bt/glass}$ versus temperature for ASI values of 1.08 to 1.18. The data are grouped according to Mg′ of biotite. The data show little to no variation of $D_F^{Bt/glass}$ over this narrow temperature interval

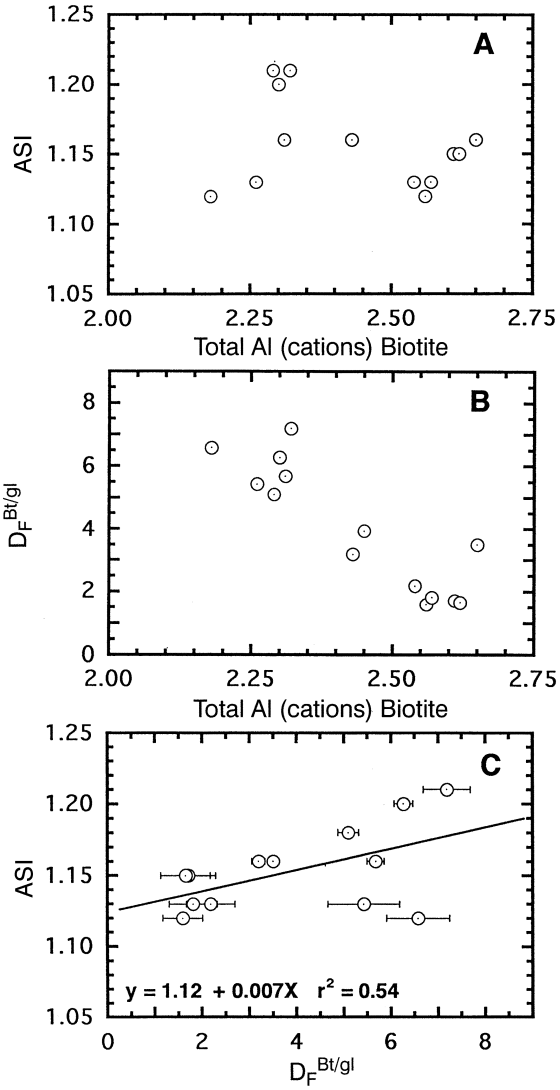

Fig. 4A Plot of total aluminum in biotite versus ASI of melt. No correlation exists between the two parameters. **B** Plot of $D_F^{Bt/glass}$ versus total aluminum in biotite. The negative correlation is probably controlled by the substitution of Mg into biotite, *not* by melt composition. **C** Plot of $D_F^{Bt/glass}$ versus ASI of melt. The positive correlation of these variables stems from reaction 2 (see text), which proceeds with increasing Mg′ of the system (melt + mica)

the assemblage Ab-Ms-Bt-Qtz ± Crd, Gt, Spl (Synpel: Icenhower and London 1993, 1995). The experiments contained melt and biotite with 1-2 w% Li_2O, and $D[Li]^{Bt/melt}$ varied from 1.0 to 1.7 (Icenhower and London 1995). From the high Li content of the biotite we might have expected the $D_F^{Bt/melt}$ to be higher in the Synpel system (e.g., Muñoz 1984) rather than lower. The only significant difference between experiments with Synpel and Spor Mountain at $Mg' = 40-50$ is that the Li content and ASI values of melt are much higher in the Synpel system. Though the precise reason is not clear, we hypothesize that the combination of Li and especially high ASI decrease the activity coefficient of F ($a_F^{Bt} = a_F^{melt}$) in the Synpel melts (e.g., Manning et al. 1980) thus lowering $D_F^{Bt/melt}$. This does not contradict, nor even compare with the trends shown in Fig. 4C, wherein $D_F^{Bt/melt}$ increases with ASI. The data plotted in Fig. 4C do not include Mg′ of biotite, which increases with ASI of melt by exchange reaction 2 and which appears to be one of the most important controls on $D_F^{Bt/melt}$.

Comparison of $D_F^{Bt/melt}$ with other experimental data

Values of $D_F^{Bt/melt}$ determined from experiments (Patiño-Douce and Johnston 1991; LaTourrette et al. 1995; Righter and Carmichael 1996) overlap with or lie below our results (Fig. 6). Experiments by Righter and Carmichael (1996) utilized lamprophyre, and those by Patiño-Douce and Johnston (1991) were at H_2O contents of melt far below saturation. All of these experiments were conducted at higher pressures and temperatures than ours. Considering these differences, the correspondence of all the experimental values for $D_F^{Bt/melt}$ is surprisingly good.

Comparison of $D_F^{Bt/melt}$ with natural volcanics

Figure 6 also illustrates the apparent $D_F^{Bt/melt}$ values obtained on natural compositions from Twin Peaks,

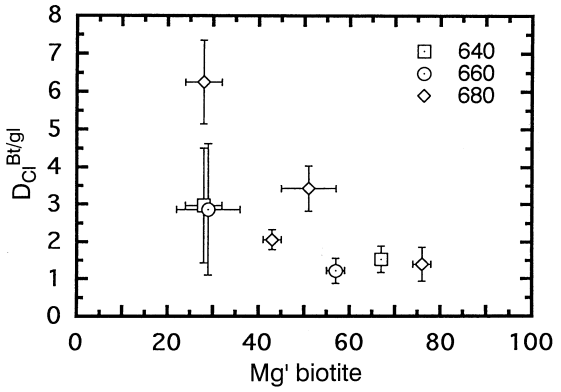

Fig. 5 Plot of $D_{Cl}^{Bt/glass}$ versus Mg′ of biotite; 1σ error bars on the parameters are included

Utah (Crecraft et al. 1981), Taylor Creek, New Mexico (Webster and Duffield 1991), the Bishop Tuff, California (Mahood and Hildreth 1983), Macusani volcanics, Peru (Pichavant et al. 1987), and the Honeycomb Hills, Utah (Congdon and Nash 1991). Clearly, most values from natural volcanic samples plot well above the experimental result from Fig. 3A, and hence a detailed examination of this discrepancy is warranted.

We focus our attention on the fluorosiderophyllite micas studied by Nash (1993) from the Honeycomb Hills rhyolite, Utah (USA). From our data, $D_F^{Bt/melt}$ approaches zero as Mg′ goes to zero, which is compatible with previous studies that demonstrated (using a natural sample base) or predicted Fe-F avoidance in biotite (e.g., Kalinichenko et al. 1975; Sanz and Stone 1983; Mason 1992). For the Honeycomb Hills samples, however, $D_F^{Bt/melt}$ ranges from 5 to 16 at Mg′ ≈ 0. Nash (1993) reported only one analysis of Fe^{3+}/Fe^T, in biotite sample #32, for which 23 % of total Fe is ferric. This ratio plots 2 log units above NNO in the experiments of Righter and Carmichael (1996), which is entirely consistent with Nash's (1993; also Congdon and Nash 1991) estimate of an f_{O_2} of ~ 2 log units above NNO. Nash (1993) attributed F-rich domal biotite ($D_F^{Bt/melt} = 16$), with notably F-rich rims and F-poorer cores, to degassing of magma prior to eruption. Because of the comparative nonvolatility of F in melt (e.g., Manning 1981, Dingwell et al. 1985; Webster 1990), degassing of H_2O would indeed promote growth or exchange of biotite to F-richer rims. Biotite from earlier-erupted tuffs is thought to preserve pre-eruptive volatile contents (Nash 1993), but it still plots well above our data with $D_F^{Bt/melt} = 5$. We speculate, therefore, that oxidation of Fe in the octahedral layer of biotite might promote increased incorporation of F, as for example by:

$$Fe^{2+}OH^-_{bt} + F_2O_{-1} = Fe^{3+}F^-_{2\,bt} + 1/2H_{2melt\ or\ vapor}, \quad (3a)$$

which is a combination of the oxidation-deprotonation reaction

$$(Fe^{3+}O)(Fe^{2+}OH)_{-1} \quad (3b)$$

and fluorine-oxygen exchange

$$F_2O_{-1}. \quad (3c)$$

Whether this hypothetical exchange occurs or not, it is important to note that the biotite compositions reported by Nash (1993) apparently lie far from the annite-siderophyllite join with very high Fe^{3+}. Oxidation to Fe^{3+} at high f_{O_2} (perhaps late-magmatic or even post-eruptive, and not reflected by less reactive oxides) may be endemic to biotite from other volcanic centers, including those plotted on Fig. 6, although the precise values of Fe^{3+}/Fe^T in biotite are not reported or known with certainty.

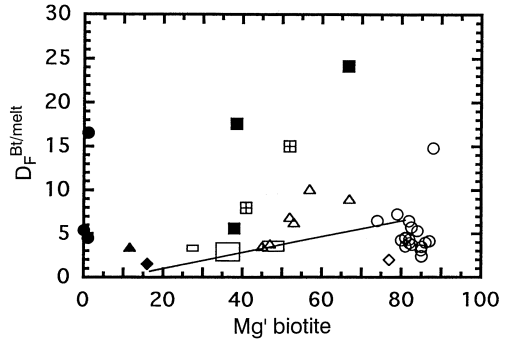

Fig. 6 Plot of $D_F^{Bt/glass}$ versus Mg′ in biotite from natural (*filled symbols*) and experimental (*open symbols*) biotite/glass pairs. *Open triangles* biotite-melt experiments (Patiño-Douce and Johnston 1991), *open circles* phlogopite-melt experiments (Righter and Carmichael 1996), *open diamond* phlogopite-melt experiments (LaTourrette et al. 1995), *filled diamond* Macusani, Peru (Pichavant et al. 1987), *filled circle* Honeycomb Hills, Utah (Congdon and Nash 1991), *filled triangle* Taylor Creek, New Mexico (Webster and Duffield 1991), *filled squares* Twin Peaks, Utah (Crecraft et al. 1981), *squares with crosses* Bishop Tuff, California (Mahood and Hildreth 1983). *Rectangles* show the range of $D_F^{Bt/glass}$ values from biotite core/melt inclusion data from three distinct rhyolite units from Morococala, Bolivia (Morgan et al. 1995). The data from Macusani, Morococala and the experiments are remarkably consistent with our calibration (*solid line*) despite differences in T, P, f_{O_2}, and X_{H_2O} (see text)

Analyses of biotite and coexisting glass from the peraluminous Macusani rhyolite, Peru (Pichavant et al. 1987) yield a value of $D_F^{Bt/melt}$ that plots on the linearly regressed fit of our experimental data (Fig. 6). Partition coefficients for Li, Rb, Cs and Ba reported by Pichavant et al. (1987) are also similar to our results (Icenhower and London 1995). In a more extensive study (Morgan et al. 1995, and work in prep), biotite from a zoned rhyolite sequence in the Morococala volcanic field, Bolivia, also contains biotite with sharply zoned F-rich rims. When compared to the compositions of melt inclusions in coexisting quartz phenocrysts, the cores of this biotite yield values of $D_F^{Bt/melt}$ that lie on our experimental curve over a range of Mg′ from 20 to 50. Obviously, with no change in Mg′, values of $D_F^{Bt/melt}$, similarly determined for the F-rich rims, trend above and away from our experimental values, as do the bulk of the data for other volcanic rocks. The Macusani and Morococala volcanics possess an S-type magmatic signature (Pichavant et al. 1987; Morgan et al. 1995), are ilmenite-dominant, and hence characteristically reduced.

In summary, we suggest that the $D_F^{Bt/melt}$ values determined on natural volcanic samples are too high due to either oxidation reactions or reequilibration of biotite with a progressively declining f_{H_2O}/f_{HF} ratio. Values of $D_F^{Bt/melt}$ determined on experimentally grown biotite on natural peralkaline compositions are similar to our results (LaTourrette et al. 1995; Righter and Carmichael 1996), but are lower, perhaps due to melt composition (Fig. 6). Our results generally overlap with $D_F^{Bt/melt}$ values determined on experimentally grown biotite on a natural peraluminous gneiss (Patino-Douce and Johnston 1991); discrepancies at a higher Mg′ values may be due to differences in X_{H_2O} between the experiments. Our results are strictly applicable only to silicic igneous magmas that are generated or crystallized at high water content (not just high a_{H_2O}), low to moderate T, and f_{O_2} of ~ FMQ to NNO.

Chlorine

Values of $D_{Cl}^{Bt/melt}$ vary between 1.2 and 6.2 (Table 4). Two of the eight experiments for which $D_{Cl}^{Bt/melt}$ were determined were doped with additional Cl (GA3-4, -5). The total Cl added is equivalent to ~2,000 – 3,000 ppm Cl, though the water/melt ratios of these experiments were high enough to remove some Cl from melt and consequently to leave the melts undersaturated in Cl (see Webster 1992). Loss of Fe to Cl-rich vapor precluded measurement of $D_{Cl}^{Bt/melt}$ values at higher total Cl content. The values of $D_{Cl}^{Bt/melt}$ derived from these experiments, however, demonstrate what might be seen as a surprisingly high compatibility of Cl for biotite.

Mason (1992, and references therein) suggested that there is a structural Mg-Cl avoidance that is complementary to Fe-F avoidance in biotite, and hence that $D_{Cl}^{Bt/melt}$ values should decrease with increasing Mg′. Our preliminary results are consistent with this trend: $D_{Cl}^{Bt/melt}$ decreases from 3 – 6 at $Mg' = 30$ to 1.4 at $Mg' = 70$.

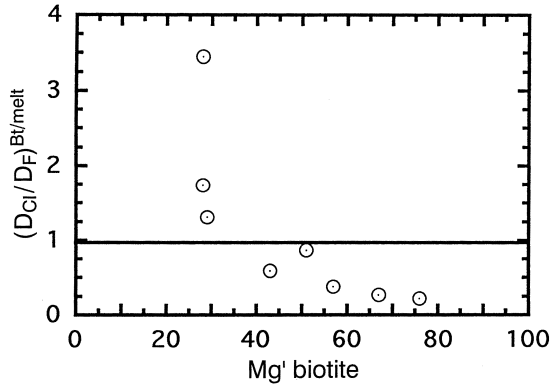

Fig. 7 Plot of $(D_{Cl}/D_F)^{Bt/glass}$ versus Mg′ of biotite

Fluorine versus chlorine

We find a cross-over in the distribution of Cl and F between biotite and melt, $D_{Cl}/D_F \cong 1$, near $Mg' = 50$ (Fig. 7). At lower Mg′ comparable to biotite from most silicic igneous rocks, $D_{Cl}/D_F > 1$ or $D_{Cl}^{Bt/melt} > D_F^{Bt/melt}$. The converse is evident ($D_{Cl}/D_F < 1$) for more magnesian biotite, but such compositions ($Mg' > 60$) would be unusual for silicic igneous rocks.

As the experimental melts produced here are undersaturated in Cl, we suggest that the reported values for both $D_F^{Bt/melt}$ and $D_{Cl}^{Bt/melt}$ are valid partition coefficients for what represent dilute solutions of these two components in biotite and melt.

Calculations of fluorine concentrations in silicic magmas

Though the Fluorine Intercept Value of Muñoz (1984) remains useful for distinguishing a relative and qualitative measure of F in igneous systems, it is desirable for reasons presented in the introduction to know or approximate the actual F-content of magma. The methods described by Muñoz and Ludington (1974) have been used – we would say misused because of assumptions involved – to estimate the actual F content of melt. Below we work through a model calculation to illustrate that, assumptions notwithstanding, the calculated values are for an HF species, which is a negligible fraction of the total F content of melt.

The calibrations of Muñoz and Ludington (1974) provide a means to calculate the activity ratio a_{H_2O}/a_{HF} of aqueous vapor in equilibrium with biotite as functions of T and biotite composition:

$$\log K = 2100/T + 1.523X_{Mg} + 0.416X_{Ann} + 0.200X_{Sid}, \text{ and} \quad (4a)$$

$$\log K = \log(X_F^{bt}/X_{OH}^{bt}) + \log(f_{H_2O}^{fl}/f_{HF}^{fl}), \text{ where} \quad (4b)$$

$$X_{Sid} = [(3 - Si/Al)/1.75] \cdot [1 - X_{Mg}], \text{ and} \quad (4c)$$

$$X_{Ann} = 1 - (X_{Mg} + X_{Sid}) \quad (4d)$$

in which X_{Sid} and X_{Ann} are the mole fraction of the siderophyllite and annite components of biotite, respectively. A model calculation, presented below for biotite compositions from SM-9 (Table 2), indicates that the amount of HF in melt estimated by this method is, as expected, very small (cf., Schaller et al. 1992).

The assumptions that previous investigators have employed include:

$$a_{HF}^{bt} = a_{HF}^{fl} = a_{HF}^{melt}, \text{ and} \quad (5a)$$

$$a_{H_2O}^{bt} = a_{H_2O}^{fl} = a_{H_2O}^{melt} \quad (5b)$$

where a, bt and fl stand for activity, biotite and fluid, respectively, for an H_2O-saturated magma in which equilibrium exists between biotite, fluid, and melt. If the ratio of the standard state fugacities of components in fluid is set equal to unity (for lack of a better value for f_{HF}° at elevated P):

$f^{\circ}_{HF}/f^{\circ}_{H_2O}{}^{fl} = 1$, then: (6)

$$a_{H_2O}/a^{fl}_{HF} = (f_{H_2O}/f^{\circ}_{H_2O})/(f_{HF}/f^{\circ}_{HF})^{fl} = f_{H_2O}/f^{fl}_{HF} \quad (7a)$$

where f and f° stand for the fugacity and the standard-state fugacity (in this case, pure component at P and T), respectively. The fugacity ratio for H_2O and HF in fluid can be estimated by Eqs. 4a, b. By Eqs. 5a,b and if the activity coefficients for H_2O and HF are equal (i.e., $\gamma_{H_2O} = \gamma_{HF}$; again, an unwarranted assumption for lack of relevant data for γ_{HF}) then Eq. 7a becomes:

$$(a_{H_2O}/a_{HF})^{melt} = (X_{H_2O}/X_{HF})^{melt} \quad (7b)$$

The mole fraction of HF in melt ($X_{HF}{}^{melt}$) can be solved for if the mole fraction of H_2O in melt is known. This latter quantity can be estimated by first calculating the gram formula weight (gfw) of melt by the method of Burnham (1979). We have used the method outlined above and a gfw = 260.48 for SM-9 glass to calculate the F content of melt in experiment SM-9 as HF. For this purpose, we took the concentration of H_2O dissolved in SM-9 glass as the difference between 100 and the EMPA wt% total (or ~6 wt%), a methodology that has proven reliable with the proper EMPA conditions (Morgan and London 1996). The estimated amount of HF is ~0.02 wt%, nearly 2 orders of magnitude less than the measured value of 1.8 wt%. In this calculation, the melt was known to be saturated with H_2O at a known pressure. In the more general case, the value of X_{H_2O} in melt is nearly as enigmatic as X_{HF} unless the pressure of crystallization is established and the melt is assumed to be saturated in H_2O or a_{H_2O} can be established through mineral-melt equilibria.

Applications of this work

The results presented here may serve several purposes. One is to use these partition coefficients when modeling or estimating the volatile content of hydrous magmas that have not been extensively oxidized. The significance of Mg′ and F in biotite is now well established, and should dramatically affect the F content of melts. It is evident that the equilibration of biotite with melt, e.g., at anatexis, will liberate more fluorine to melt than might have been expected. The available data on $D_F{}^{Bt/melt}$, most of which are derived from relatively dry (degassed) and oxidized volcanic magmas (or at least the biotite appears to be oxidized, even if other mineral indicators reflect lower f_{O_2}), are mostly not applicable. The disparity between the values of $D_F{}^{Bt/melt}$ derived from experiments (ours and others cited) and volcanic rocks (Fig. 6) reveals that the volatile history, at least recorded by biotite, in volcanics is nothing like that for hydrous plutonic igneous magmas. Whereas some minerals from volcanics undoubtedly preserve a record of conditions and growth in deeper magma chambers, most volcanic biotite apparently does not. The measured $D_F{}^{Bt/melt}$ values, where melt = matrix or included glass, for ilmenite-bearing S-type volcanic rocks from Peru and Bolivia (Fig. 6) show a good correspondence to our experimental values using Spor Mountain rhyolite.

We recognize that subsolidus reequilibration of micas in plutonic rocks is not only common but often incomplete and at scales too fine for detection by EMPA (e.g., see Goodman and London 1985; Ferrow et al. 1990). For biotite, one test of reequilibration might be mineral-mineral trace element partitioning, e.g., among coexisting biotite and muscovite (see Icenhower and London 1995). Nevertheless, the method of using Mg′ to estimate F content of melt is still preferable to misuse of the biotite-vapor equilibria of Muñoz and Ludington (1974), if no other reliable means is available.

The most likely application of these partition coefficients is for plutonic rocks emplaced in shallow magma chambers, such that crystallization will occur before extensive exchange reactions between biotite and melt or vapor. Under the best of circumstances, the magma will be close to H_2O saturation but will not exsolve or circulate a fluid phase that will cause extensive hydrothermal alteration. As an example, A-type granites and rhyolites are commonly characterized as F-rich (e.g., Whalen et al. 1987) despite the fact that they do not fully conserve F. Using the results presented here (Fig. 3A), Hogan and Gilbert (1993) estimated that the F content of melt from which biotite crystallized in the Mt. Scott granite sill (a typical A-type granite sheet) in Oklahoma (USA) contained ~0.8 wt% F. Some portions of the Mt. Scott are characterized by the assemblage amphibole + titanite, whereas others contain biotite + fluorite (Hogan and Gilbert 1993). Experiments using the Mt. Scott granite as starting material and replicating the best estimate of P, T, and volatile contents bracketed the reaction:

$$Ttn + 2F = Flu + Qtz + TiO_2 \quad (8)$$

and the amphibole-biotite equilibria at ~1 wt% F in melt (Price et al. 1995), which agrees reasonably well with the F content of melt estimated from the composition of biotite. The fact that many A-type granites have epizonal features (e.g., Anderson and Bender 1989) suggests that this method may be useful in determining F contents in numerous plutons.

Appendix

Electron microprobe analyses of glasses utilized two separate beam conditions in each analysis to determine major and minor element oxide concentrations. The first condition consists of a 15 μm spot size, a current of 2 nA measured at the Faraday cup, and an accelerating potential of 20 kV. These conditions minimized K and Na migration (Morgan and London 1996). The second condition consists of a 15 μm spot size, a current of 20 nA, and an accelerating potential of 20 kV. Two-sigma lower limits of detection (L.L.D.s), diffracting crystals, and counting times on peak positions are tabulated below:

Condition 1				Condition 2			
Element	L.L.D.	Crystal	Time	Element	L.L.D.	Crystal	Time
	(wt%)		(s)		(wt%)		(s)
SiO_2	0.11	TAP	90	FeO	0.02	LiF	20
Al_2O_3	0.07	TAP	80	TiO_2	0.04	LiF	20
Na_2O	0.07	TAP	10	NiO	0.04	LiF	20
K_2O	0.06	PET	15	Rb_2O	0.05	TAP	20
				MnO	0.04	LiF	10
				BaO	0.13	LiF	10
				Cs_2O	0.11	LiF	20
				P_2O_5	0.03	TAP	10
				MgO	0.02	TAP	10
				F	0.17	TAP	40
				SrO	0.07	PET	30
				CaO	0.07	PET	10
				Cl	0.01	PET	60

Acknowledgements This work constitutes a portion of the dissertation of JPI. Support for this research was provided to DL by an NSF-EPSCoR contract EHR-9108771 in conjunction with collaborative research with the University of Tulsa, and NSF grant EAR-9625517 to D.London and M.B. Wolf. The Electron Microprobe Laboratory was created by grant DE-FG22-87FE1146 to DL from the United States Department of Energy, and experimental facilities were established and maintained by grants EAR-8516753, EAR-8720498, and EAR-8821950 to DL from the National Science Foundation. We thank George Morgan for his considerable help with the microprobe analyses, and Jim Webster for providing samples of the Spor Mountain rhyolite. Review comments from Tom Dewers, John Hogan, Mike Wolf, and GCA reviewers Jim Webster and Eric Christiansen are much appreciated.

References

Anderson JL, Bender EE (1989) Nature and origin of Proterozoic A-type granitic magmatism in the southwestern United States. Lithos 23: 19–52

Anfiligov VN, Glyuk DS, Trufanvova LG (1973) Phase relations in the interaction between granite and sodium fluoride at water vapor pressure of 1000 mg/cm^2. Geokhimiya 1: 44–48

Baker LL, Rutherford MJ (1996) The effect of dissolved water on the oxidation state of silicic melts. Geochim Cosmochim Acta 60: 2179–2187

Barbarin B (1996) Genesis of the two main types of peraluminous granitoids. Geology 24: 295–298

Barnes HL (1979) Solubilities of ore minerals. In: Barnes HL (ed) Geochemistry of hydrothermal ore deposits, 2nd edn. John Wiley and Sons, New York, pp 404-460

Burnham CW (1979) The importance of volatile constituents. In: Yoder HS Jr (ed) The evolution of igneous rocks: fiftieth anniversary perspectives. Princeton University Press, New York, pp 439–482

Burt DM, Bikun JV, Christiansen EH (1982) Topaz rhyolites – distribution, origin, and significance for exploration. Econ Geol 77: 1818–1836

Chou I-M (1987) Oxygen buffer and hydrogen sensor techniques at elevated pressures and temperatures. In: Ulmer GC, Barnes HL (eds) Hydrothermal experimental techniques. John Wiley and Sons, New York, pp 61–99

Christiansen EH, Bikun JV, Burt DM (1980) Petrology and geochemistry of topaz rhyolites, western United States. US Dept Energy Open-File Report GJBX-225, 80: 37–122

Christiansen EH, Bikun JV, Sheridan MF, Burt DM (1984) Geochemical evolution of topaz rhyolites from the Thomas Range and Spor Mountain, Utah. Am Mineral 69: 223–236

Congdon RD, Nash WP (1991) Eruptive pegmatite magma: rhyolite of the Honeycomb Hills, Utah. Am Mineral 76: 1261–1278

Crecraft HR, Nash WP, Evans SH Sr (1981) Late Cenozoic volcanism at Twin Peaks, Utah: geology and petrology. J Geophys Res 86: 10303-10320

Dachs E (1994) Annite stability revised. I. Hydrogen-sensor data for the reaction annite = sanidine + magnetite + H_2. Contrib Mineral Petrol 117: 229–240

Dachs E Benisek A (1995) The stability of annite + quartz: reversed experimental data for the reaction 2 annite + 3 quartz = 2 sanidine + 3 fayalite + 2 H_2O. Contrib Mineral Petrol 121: 380–387

Dingwell DB (1985) The structure and properties of fluorine-rich silicate melts: implications for granite petrogenesis (abstract). In: Taylor RP, Strong DF (eds) Granite-related mineral deposits. Can Inst Mining, Extended Abstracts Conference on Granite-Related Mineral Deposits, Halifax, pp 72–81

Dingwell DB (1987) Melt viscosities in the system $NaAlSi_3O_8$-H_2O-F_2O_{-1}. In: Mysen BO (ed) Magmatic processes: physicochemical principles. (Geochem Soc Spec Pub no. 1), Geochemical Society, Penn State Univ, pp 423–431

Dyar MD (1990) Mössbauer spectra of biotite from metapelites. Am Mineral 75: 656–666

Ferrow E, London D, Goodman KS, Veblen DR (1990) Sheet silicates of the Lawler Peak granite, Arizona: chemistry, structural variations, and exsolution. Contrib Mineral Petrol 105: 491–501

Finch AA, Parsons I, Mingard SC (1995) Biotites as indicators of fluorine fugacities in late-stage magmatic fluids: the Gardar Province of south Greenland. J Petrol 36: 701–728

Goodman KS, London D (1985) Significance of muscovite in the Lawler Peak granite, Yavapai County, Arizona (abstract). EOS Trans Am Geophys Union 66: 1147

Guidotti CV (1984) Micas in metamorphic rocks. In: Bailey SW (ed) Micas (Reviews in Mineralogy vol. 13). Mineralogical Society of America, Washington DC, pp 357–467

Hogan JP, Gilbert MC (1993) The role of fluorine in crystallization of A-type sheet granites, Wichita Mountains Oklahoma (abstract). Geol Soc Am Abstr Prog 25: 372

Huebner JS, (1971) Buffering techniques for hydrostatic systems at elevated pressures. In: Ulmer GC, (ed) Research techniques for high pressure and high temperature. Springer, Berlin, pp 123–177

Icenhower JP, London D (1993) An experimental study of the partitioning of fluorine between biotite and silicic melts (abstract). Geol Soc Am Abstr Prog 25: 372

Icenhower JP, London D (1995) An experimental study of element partitioning among biotite, muscovite and coexisting peraluminous silicic melt at 200 MPa (H_2O). Am Mineral 80: 1229–1251

Kalinichenko AM, Matyash IV, Khomyak TP, Pavlishin VI (1975) Distribution of octahedral cations in biotites according to the data of proton magnetic resonance. Geochem Int 12: 18–24

Keppler H, (1993) Influence of fluorine on the enrichmen t of high field strength trace elements in granitic rocks. Contrib Mineral Petrol 114: 479–488

LaTourrette T, Hervig RL, Holloway JR (1995) Trace element partitioning between amphibole, phlogopite, and basanite melt. Earth Planet Sci Lett 135: 13–30

London D (1987) Internal differentiation of rare-element pegmatites: effects of boron, phosphorus, and fluorine. Geochim Cosmochim Acta 51: 403–420

Mahood G, Hildreth W (1983) Large partition coefficients for trace elements in high-silica rhyolites. Geochim Cosmochim Acta 47: 11–30

Manning DAC (1981) The effect of fluorine on liquidus phase relationships in the system Qz-Ab-Or with excess water at 1 kb. Contrib Mineral Petrol 76: 206–215

Manning DAC, Hamilton DL, Henderson CMB, Dempsey MJ (1980) The probable occurrence of interstitial Al in hydrous, F-bearing and F-free aluminosilicate melts. Contrib Mineral Petrol 75: 257–262

Mason RA (1992) Models of order and iron-fluorine avoidance in biotite. Can Mineral 30: 343–354

Morgan GB VI, London D (1996) Optimizing the electron microprobe analysis of hydrous alkali aluminosilicate glasses. Am Mineral 81: 1176–1185

Morgan GB VI, London D, Luedke RG (1995) Melt inclusion, matrix glass, and mineral compositions from a zoned S-type peraluminous rhyolite suite, Morococala Volcanic Field, Bolivia (abstract). In: Brown M, Piccolli PM (ed) The origin of granites and related rocks, 3rd Hutton Symposium. US Geol Surv Circ 1129: 99–100

Muñoz JL (1984) F-OH and Cl-OH exchange in micas with applications to hydrothermal ore deposits. In: Bailey SW (ed) Micas. (Reviews in Mineralogy 13) vol. Mineralogical Society of America, Washington DC, pp 469–493

Muñoz JL, Ludington SD (1974) Fluoride-hydroxyl exchange in biotite. Am J Sci 274: 396–413

Nash WP (1993) Fluorine iron biotite from the Honeycomb Hills rhyolite, Utah: the halogen record of decompression in a silicic magma. Am Mineral 78: 1031–1040

Patiño-Douce AE, Johnston AD (1991) Phase equilibria and melt productivity in the pelite system: implications for the origin of peraluminous granitoids and aluminous gneisses. Contrib Mineral Petrol 107: 202–218

Pichavant M, Valencia-Herrera J, Boulmier S, Briqueu L, Joron JL, Juteau M, Marin L, Michard A, Sheppard S, Treuil M, Vernet M (1987) The Macusani glasses, SE Peru: evidence of chemical fractionation in peraluminous magmas. In: Mysen BO (ed) Magmatic processes: physicochemical principles. (Geochem Soc Spec Pub 1). Geochemical Society, Penn State Univ, pp 359–373

Peterson JW, Chacko T, Kuehner SM (1991) The effects of fluorine on the vapor-absent melting of phlogopite + quartz: implications for deep-crustal processes. Am Mineral 76: 470–476

Price JD, Hogan JP, Gilbert MC, London D, Morgan GB VI (1995) Fluorine in A-type granites: experimental studies of the Mount Scott granite (abstract). Geol Soc Am Abstr Prog 27: 431–432

Puziewicz J, Johannes W (1990) Experimental study of biotite-bearing system under water-saturated and water-undersaturated conditions. Contrib Mineral Petrol 104: 397–406

Redhammer GJ, Beran A, Dachs E, Amthauer G (1993) A Mössbau er and X-ray diffraction study of annites synthesized at different oxygen fugacities and crystal chemical implications. Phys Chem Mineral 20: 382–394

Righter K, Carmichael ISE (1996) Phase equilibria of phlogopite lamprophyres from western Mexico: biotite-liquid equilibria and *P-T* estimates for biotite-bearing igneous rocks. Contrib Mineral Petrol 123: 1–21

Robert J-L, Maury RC (1979) Natural occurrence of a (Fe, Mn, Mg) tetrasilicic potassium mica. Contrib Mineral Petrol 68: 117–123

Sanz J, Stone WEE (1983) NMR applied to minerals. IV . Local order in the octahedral sheet of micas: Fe-F avoidance. Clay Miner 18: 187–192

Schaller T, Dingwell DB, Keppler H, Knoller W, Merwin L, Sebald A (1992) Fluorine in silicate glasses: a multinuclear nuclear magnetic resonance study. Geochim Cosmochim Acta 56: 701–707

Seifert F, Schreyer W (1971) Synthesis and stability of micas in the system K_2O-MgO-SiO_2-H_2O and their relations to phlogopite. Contrib Mineral Petrol 30: 196–215

Skjerlie KP, Johnston AD (1992) Vapor-absent melting at 10 kbar of a biotite- and amphibole-bearing tonalitic gneiss: implications for the generation of A-type granites. Geology 20: 263–266

Villaseca C, Barbero L (1994) Chemical variability of Al-Ti-Fe-Mg minerals in peraluminous granitoid rocks from Central Spain. Eur J Mineral 6: 691–710

Webster JD (1990) Partitioning of F between H_2O and CO_2 fluids and topaz rhyolite melt. Contrib Mineral Petrol 104: 424–438

Webster JD (1992) Fluid-melt interactions involving Cl-rich granites: Experimental study from 2-8 kbar. Geochim Cosmochim Acta 56: 659–678

Webster JD, Duffield WA (1991) Volatiles and lithophile elements in Taylor Creek Rhyolite: constraints from glass inclusion analysis. Am Mineral 76: 1628–1645

Webster JD, Holloway JR (1988) Experimental constraints on the partitioning of Cl between topaz rhyolite melts and H_2O and H_2O + CO_2 fluids: new implications for granitic differentiation and ore deposition. Geochim Cosmochim Acta 52: 2091–2105

Webster JD, Holloway JR, Hervig RL (1987) Phase equilibria of a Be, U and F-enriched vitrophyre from Spor Mountain, Utah. Geochim Cosmochim Acta 51: 389–402

Whalen JB, Currie KL, Chappell BW (1987) A-type granites: geochemical characteristics, discrimination, and petrogenesis. Contrib Mineral Petrol 95: 407–419

Zhu C, Sverjensky DA (1992) F-Cl-OH partitioning between biotite and apatite. Geochim Cosmochim Acta 56: 3435–3467